# We are IntechOpen, the world's leading publisher of Open Access books Built by scientists, for scientists

**4,800**
Open access books available

**122,000**
International  authors and editors

**135M**
Downloads

Our authors are among the

**154**
Countries delivered to

**TOP 1%**
most cited scientists

**12.2%**
Contributors from top 500 universities

**WEB OF SCIENCE**™

Selection of our books indexed in the Book Citation Index
in Web of Science™ Core Collection (BKCI)

## Interested in publishing with us?
## Contact book.department@intechopen.com

Numbers displayed above are based on latest data collected.
For more information visit www.intechopen.com

# Structural, Optical and Electrical Properties of Undoped and Doped ZnO Thin Films

*Lourdhu Bruno Chandrasekar, S. Nagarajan,*
*Marimuthu Karunakaran and T. Daniel Thangadurai*

## Abstract

ZnO, which has high electrochemical stability, wide band gap energy, large excitonic binding energy, intense near band excitonic emission and is non-toxic, have potential applications in all fields. This chapter reviews the structural, optical and electrical properties of undoped and doped ZnO thin films. The type of doping highly influences the structural properties such as grain size, texture coefficient and unit cell properties. The dopants of transition metal and nonmetals have unique characteristics. Moreover, mono-doping and co-doping encourage this research. The optical properties such as bandgap, charge carrier concentrations and transmissions of the films depend on the doping as well as the preparation condition of the films. The effect of doping on its properties is also discussed.

**Keywords:** structural, electrical, ZnO, doping

## 1. Introduction

Recent developments in low-dimensional semiconductors create a wide range of applications and opportunities for the fabrication of varieties of devices for the future. The confinement of the charge carrier results in providing unique properties to the materials which are size dependent. Transparent conducting oxides such as CuO, $Sn_2O$ and ZnO have potential applications in the field of photovoltaic and sensing systems. Out of many transparent conducting oxides, ZnO has unique properties such as high excitation binding energy at room temperature, chemical and thermal stability, n-type semiconductor, biocompatibility, etc. [1, 2]. They have a wide range of applications including antibacterial activity, photodetectors, memory applications, LED, solar cell, gas sensors and acoustic wave devices [3–11]. The interests in the ZnO thin films can be viewed easily by the millions of research articles on ZnO thin films prepared under different conditions like substrate temperature, pH value of the solution, doping concentration and annealing temperature. Spray pyrolysis, successive ionic layer adsorption and reaction (SILAR), magnetron sputtering, sol-gel spin coating, pulsed laser deposition, atomic layer deposition and chemical bath deposition are some of the few methods available to prepare the undoped and doped ZnO films [10, 12–17]. Recently, co-doped ZnO such as Al-In-doped ZnO films and F-In-doped ZnO films, ZnO-based thin film transistors, field emission display, white light emission and p-type ZnO encourage
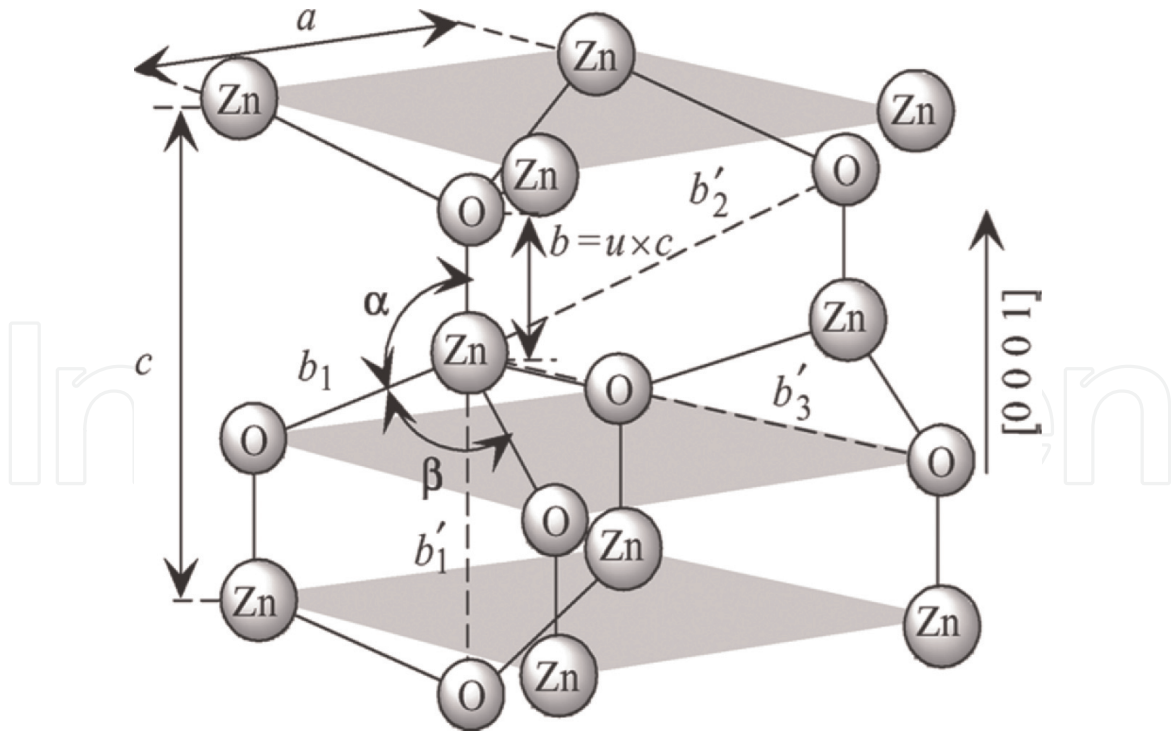
**Figure 1.**
*Representation of wurtzite geometry ZnO unit cell.*

this research [18–22]. This chapter provides an insight into the structural, optical and electrical properties of undoped and doped wurtzite geometry ZnO thin films which are quite important for future potential device designs. **Figure 1** shows the representation of wurtzite geometry ZnO. The lattice constants '*a*' and '*c*' are related by the d-spacing of the corresponding Miller indices (*hkl*) by $d^{-2} = \frac{4}{3}\left(\frac{h^2+hk+k^2}{a^2}\right) + \frac{l^2}{c^2}$. The ideal value of lattice constants '*a*' and '*c*' are, respectively, 0.325 and 0.521 nm. The bond length is calculated as $b = \sqrt{\frac{1}{3}a^2 + (0.5-u)^2 c^2}$, where *u* is 0.25 + {$0.33a^2/c^2$}. The bond angles are $\alpha = \frac{\pi}{2} + arccos\left[\left(\sqrt{1 + 3(c/a)^2 (0.5-u)^2}\right)^{-1}\right]$ and $\beta = 2\ arcsin\left[\left(\sqrt{\frac{4}{3} + 4(c/a)^2 (0.5-u)^2}\right)^{-1}\right]$ [23, 24]. It has 3.37 eV band gap at room temperature and possesses both paramagnetic and ferromagnetic nature according to the type of doping.

The structural properties of the ZnO thin films are seldom affected during doping up to certain atomic concentrations, and the structure gets modified slightly due to doping. The structural properties of the doped ZnO thin films are given in Section 2. The changes in optical properties, mainly the band gap variation, are discussed in Section 3. The variations in electrical properties of the undoped and doped thin films are presented in Section 4 followed by the conclusion.

## 2. Structural properties

Co-doped ZnO thin film is used in transparent electrode applications, where indium-tin-oxide was used in the past. For example, spray pyrolysis is employed to prepare the Co-doped ZnO thin film, and the structural properties are analysed with different doping concentrations [1]. The XRD studies reveal that the wurtzite nature of the materials is retained. The Miller indices (100), (002) and (101)

became dominant than (102), (110) and (103) which are dominant for the pristine system. The doping concentration influences the relative intensity observed between the planes (100), (002) and (101). The intensity of (100) peak is maximum when the doping concentration is 0%, and the intensity of (101) peak enhances than (100) peak when the doping concentration is 4%. The variation has been speculated. Nonsystematic variation of grain size is observed as a function of doping concentration. This is because of the fact that the grain size not only depends on the doping concentration but also depends on the crystallographic axes. The packing fraction decreases from 1.612 to 1.602 as the doping concentration increases from 0 to 4% (atomic doping concentration). **Figure 2** shows the grain size and the packing fraction of Co-doped ZnO thin film as a function of Co doping concentration.

Singh et al. reported the Fe- and Ge-doped ZnO thin films prepared by pulsed laser deposition method [25]. The undoped and doped ZnO ($Zn_{0.98}Ga_{0.02}O$ and $Zn_{0.98}Fe_{0.02}O$) thin films show a strong reflection from (002) plane. The grain size corresponds to this miller plane and increases when Ga is doped, and the same decreases when Fe is doped, compared with the undoped ZnO. Moreover, Ga doping increases the texture of the material but decreases the c-lattice parameter. But this situation is reversed due to the doping of Fe. That is, the doping of Fe in ZnO deteriorates the crystalline nature of the material and the c-lattice parameter increases. The same result is obtained when yttrium (Y) is doped in ZnO thin film prepared by sol-gel technique [26]. The reason is due to the fact that ionic radii of $Fe^{2+}$ and $Y^{3+}$ are greater than the ionic radii of $Zn^{2+}$. In both cases, the addition of either Fe or Y ion shifts the (002) miller plane to the lower angle side. The doping of $Y^{3+}$ in $Zn^{2+}$ lattice increases the c-lattice parameter from 5.205 to 5.247 Å linearly as the function of doping concentration.

The effect of Ni doping in ZnO thin film is reported by Yilmaz [27]. All the films have c-axis orientation which is confirmed by the (002) peaks. The intensity of (002) peak decreases when the doping concentration of Ni increases. The lattice constants are nearly equal irrespective of Ni doping. The full-width at half-maximum (FWHM) increases from 0.266 to 0.344° which indicates that the grain size decreases as the doping of Ni increases. **Figure 3** shows the Ni doping concentration vs. the full-width at half-maximum of the maximum intensity peak. **Figures 4** and **5** indicate the grain size and the dislocation density of the prepared films as a function of doping. The results clearly indicate that the microstructural properties of Ni-doped ZnO thin films are highly influenced by the doping concentration.
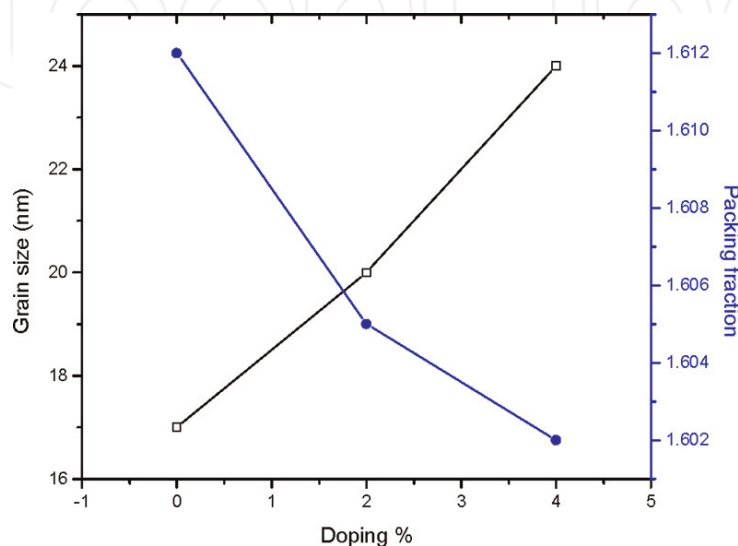


**Figure 2.**
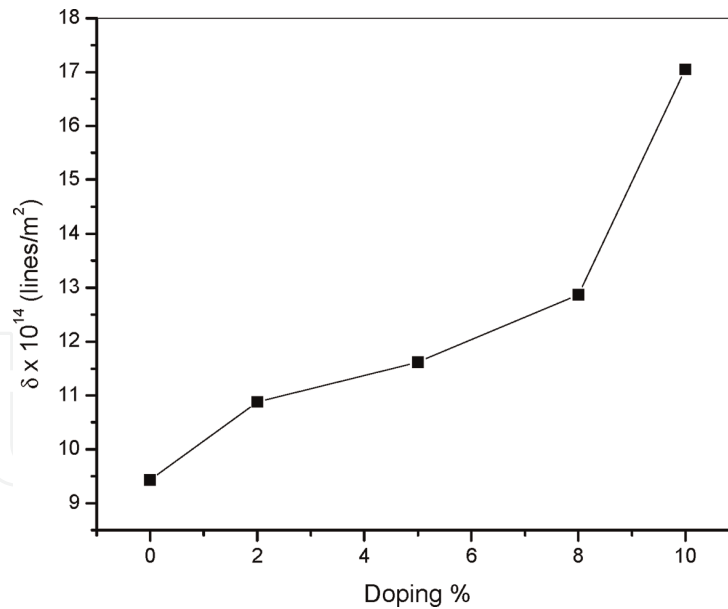*'Co' doping concentration vs. grain size and packing fraction.*
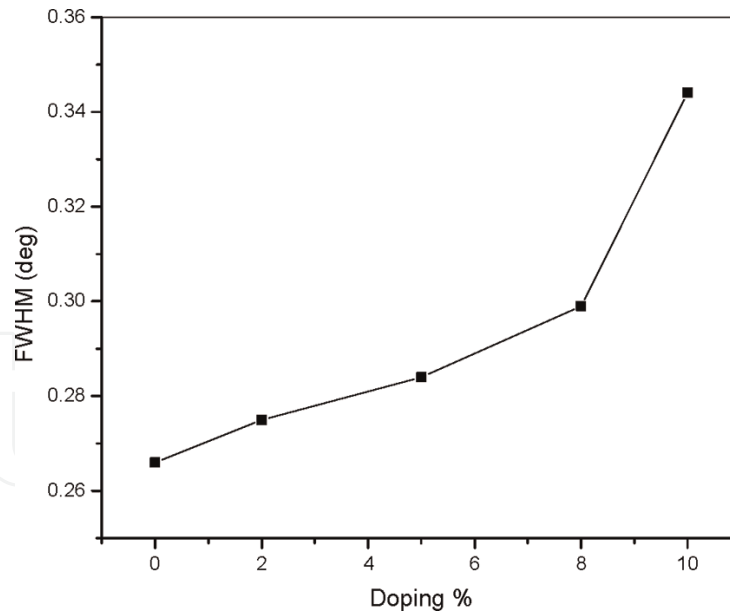
**Figure 3.**
*'Ni' doping concentration vs. FWHM.*
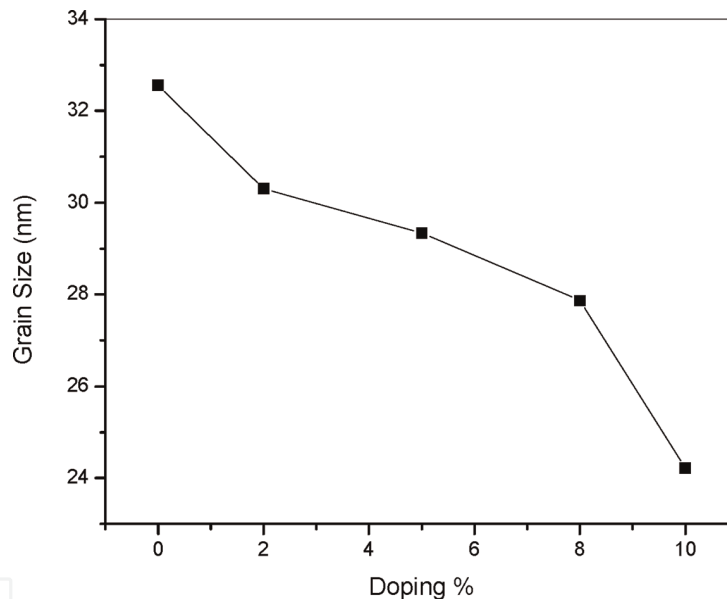


**Figure 4.**
*'Ni' doping concentration vs. grain size.*

Ni-doped ZnO thin films are prepared by a modified SILAR method and are reported by Karunakaran et al. [28]. The microstructural properties are analysed as a function of the concentration of nickel sulphate (source material for nickel) and the annealing temperature of the films. As the nickel sulphate concentration changes from 5 to 10 mM, the grain size increases from 29.5 to 44.6 nm. The miller plane (002) has high intensity when the concentration of nickel sulphate is 5 and 10 mM. However, the dominant peak orientation shifts from (002) plane to (101) plane with concentration 15 mM. The annealing increases the crystalline size of the films. The as-deposited films have the average grain size of 45.2 nm, whereas the average grain size is 48.2, 49.7 and 52.8 nm when the films are annealed at 200, 300 and 400°C for 60 min in air, respectively.

Al-doped ZnO thin films, which are prepared by SILAR method, show a redshift towards a higher diffraction angle in the XRD pattern [29]. The line width of the

**Figure 5.**
*'Ni' doping concentration vs. dislocation density.*

preferred orientation for the undoped ZnO film is 0.18°, and it is 0.21° for Al-doped ZnO films. It is clear evidence that the average grain size decreases from 46 to 39 nm due to the doping of Al. This is due to the contraction of the unit cell and Zn ions which have radius 0.74 Å is replaced by the Al ions (radius 0.51 Å). The absence of the peak (103) in the undoped sample becomes considered as the doping concentration increases. This kind of results is reported in Sr-doped ZnO thin films [16]. The grain size changes from 82 to ~28 nm when the ZnO is doped with Sr. In the Al-doped ZnO films, which are prepared by sol-gel dip coating method, the peak (002) is dominant and becomes more dominant as the concentration of Al increases, but the intensity of the peak deteriorates when 'Al' concentration becomes 10% [30].

The position of the peak (002) shifts to a lower angle side as the doping concentration increases, and it is shown in **Figure 6**. The peak (103) is dominant in the
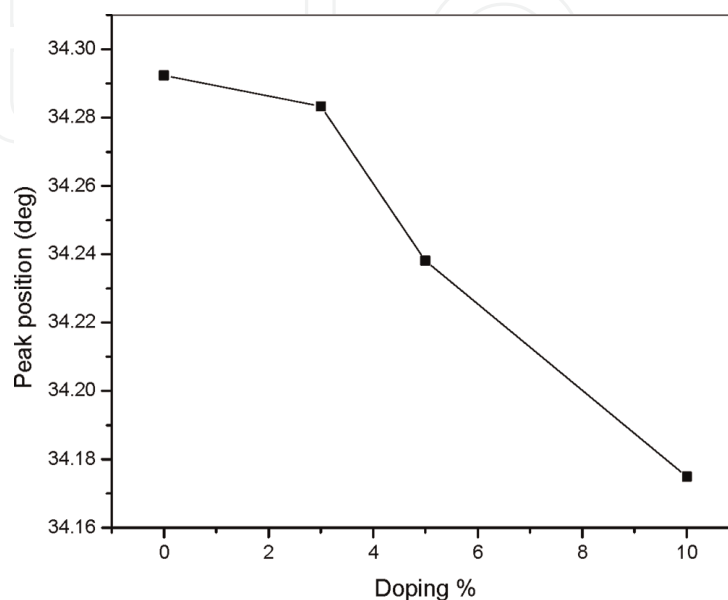


**Figure 6.**
*'Al' doping concentration vs. peak position.*

5

| 'Al' concentration | Crystallite size from topographical analysis (nm) | Crystallite size corresponds to (002) from XRD (nm) |
|---|---|---|
| 0 | 26.0 | 20.9 |
| 3 | 27.9 | 16.4 |
| 5 | 33.7 | 14.0 |
| 10 | 31.5 | 16.4 |

**Table 1.**
*Crystallites size of 'Al'-doped ZnO films.*
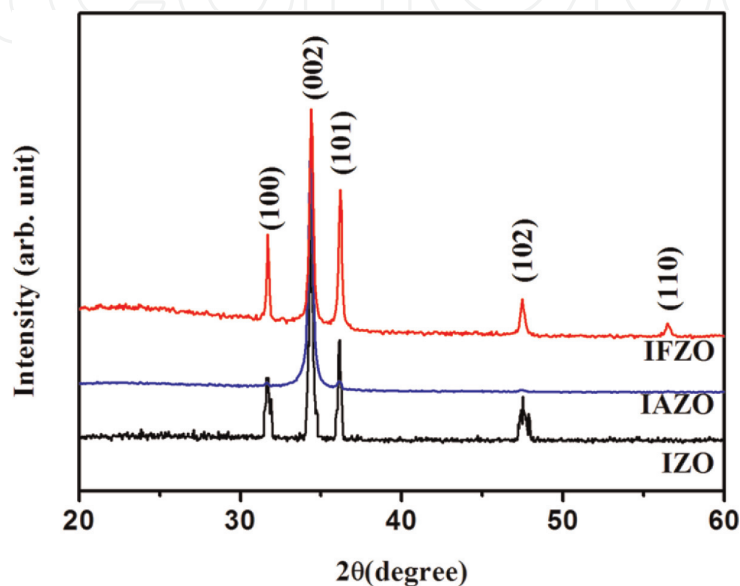


**Figure 7.**
*XRD pattern of IFZO, IAZO and IZO [18].*

undoped films and has a negligible intensity as the concentration of 'Al' increases. The crystallite size of the films varies irregularly as the doping of 'Al' concentration changes, and the crystallite sizes are given in **Table 1**.

Recently, co-doped ZnO (In-Al-co-doped ZnO and In-F-doped ZnO) films are prepared by spray pyrolysis technique. **Figure 6** shows the XRD pattern of In-Al--co-doped ZnO (IAZO) and In-F-doped ZnO (IFZO) as compared with In-doped ZnO (IZO) [18].

IFZO films showed a high intensity of (002) diffraction peak compared with other peaks. In addition, IAZO films show only the orientation from (002) peak, which indicates the IAZO films have high stoichiometry than IFZO films. The full-width at half-maximum of the IAZO films corresponding to the miller plane (002) is higher than IFZO films indicating that the IAZO has very low grain size than IFZO. This shows that not only the physical method but also chemical synthesis methods tailoring the structural properties of ZnO thin films with ease by altering parameters or by doping is feasible (**Figure 7**).

## 3. Optical properties

ZnO films were grown on p$^+$-Si substrates prepared by atomic layer deposition (ALD) [17]. The photoluminescence spectrum shows the peaks at 376, 426 and 500 nm when it is excited at 250 nm. The peaks at 376, 426 and 500 nm correspond

to the band gap 3.3 eV, 'band edge' excitonic states and reflections of the second-order harmonic of the excitation source, respectively. Apart from the second-order harmonic peak, the peak 'band edge' excitonic state is dominant than the peak at 376 nm. When the same film is excited at 390 nm, the peak due to 'band edge' excitonic states is observed at 418 nm. The peak intensities depend on the grown temperature of the material when excited at 250 nm, and the peak intensities remain almost constant when excited at 390 nm.

The Co-doped ZnO thin films show the increase in transmission with a high slope near the fundamental absorption edge in the region of 380–525 nm [1]. The films show high transmittance near the infra-red region. The doping of Co results in the d–d* intrionic transition in the region from 530 to 692 nm. Moreover, the transmission is 63% when the Co doping concentration is 0 and 79% when the concentration is 4%. The direct and indirect band gap of the Co-doped ZnO thin film is shown in **Figure 8**. The band gap decreases as the doping concentration of Co increases.

Siagian et al reported the variation of bandgap in Co-doped ZnO films up to the concentration of 10% [2]. The band gap decreases from 3.337 to 3.099 eV as the doping concentration changes from 0 to 10%, and it is shown in **Figure 9**. The transmittance of the films increases from 68.5 to 83.5% and then decreases as the doping concentration increases. The maximum transmission is obtained for the doping concentration of 7%. Surface roughness, oxygen deficiency and impurity centres are the reasons for a decrease in transmittance when the doping concentration of Co is greater than 7%.

More than 90% of transmittance in the visible region is obtained when Fe and Ga is doped in ZnO thin films [25]. As compared with the undoped ZnO films, Fe doping doesn't change the band gap significantly, but Ga doping increases the band gap. The effect of Ni doping in ZnO on its optical properties is reported by Yilmaz [27]. All the films have a sharp absorption edge at 370 nm. The films show high transparency in the region 550 nm and above. The band gap of the materials is found using dT/dλ and Tauc's plot. The transmission spectra and dT/dλ as a function of wavelength is shown in **Figure 10**. The bandgap of the material decreases as the doping of Ni increases. The transmission and band gap for various Ni doping concentration is given in **Table 2**. But according to the work published by
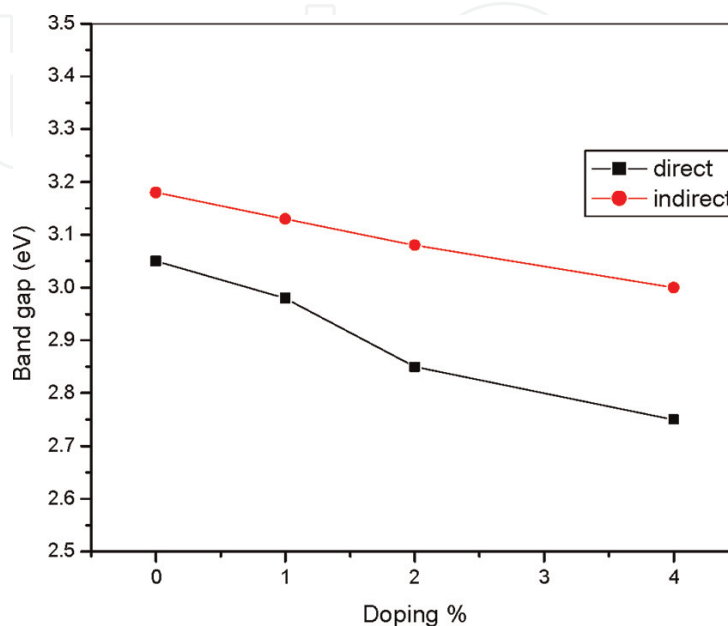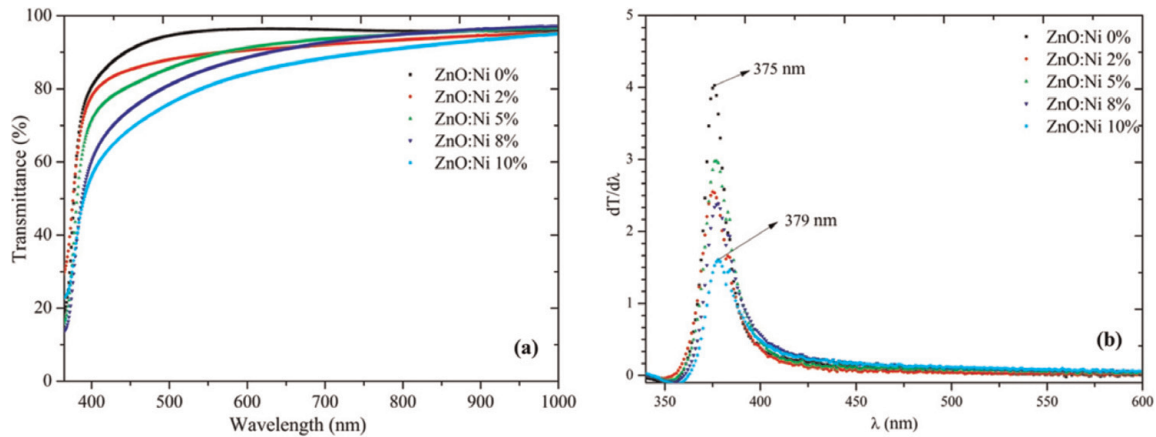


**Figure 8.**
*'Co' doping concentration vs. band gap.*
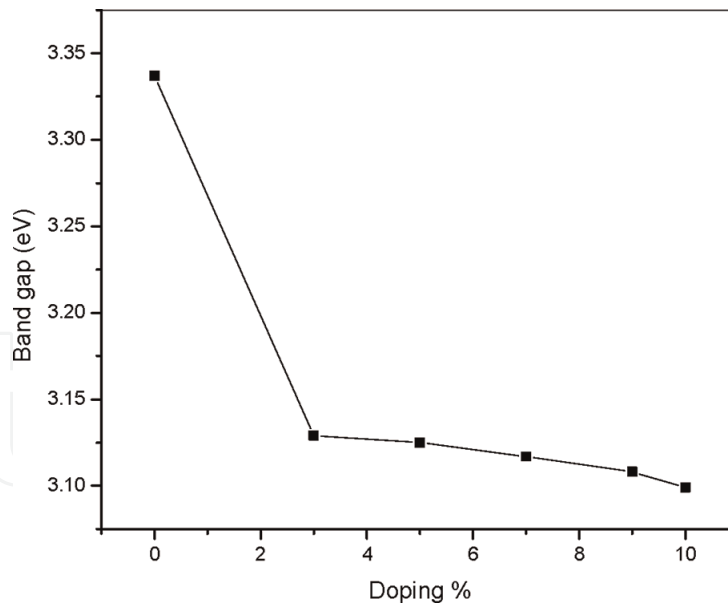
**Figure 9.**
*'Co' doping concentration vs. band gap.*



**Figure 10.**
*(a) Transmittance spectra and (b) plot of dT/dλ as a function of wavelength [27].*

| Ni doping % | Transmittance at 550 nm (%) | Band gap | |
|---|---|---|---|
| | | **dT/dλ (eV)** | **Taue's plot (eV)** |
| 0 | 90 | 3.30 | 3.27 |
| 2 | 89 | 3.30 | 3.26 |
| 5 | 88 | 3.29 | 3.23 |
| 8 | 85 | 3.28 | 3.22 |
| 10 | 80 | 3.27 | 3.19 |

**Table 2.**
*Transmittance and band gap of Ni-doped ZnO films.*

Karunakaran et al., the addition of Ni in Zn lattice increases the band gap [28]. The addition of Ni increases the refractive index and the extinction coefficient.

Y-doped ZnO films show no deep-level emission but show a strong near band edge emission which is due to the recombination of free excitons in the photoluminescence spectrum [26]. The films have a blue shift to higher energy as compared

|  | ZnO | ZnO:Sr (0.1 mM) | ZnO:Sr (1 mM) |
|---|---|---|---|
| Carrier concentration | $10.01 \times 10^{21}/cm^3$ | $27.12 \times 10^{21}/cm^3$ | $153.98 \times 10^{21}/cm^3$ |
| Refractive index | 2.34 | 2.33 | 2.32 |

**Table 3.**
*Carrier concentration and refractive index of Sr-doped films compared with undoped ZnO films.*
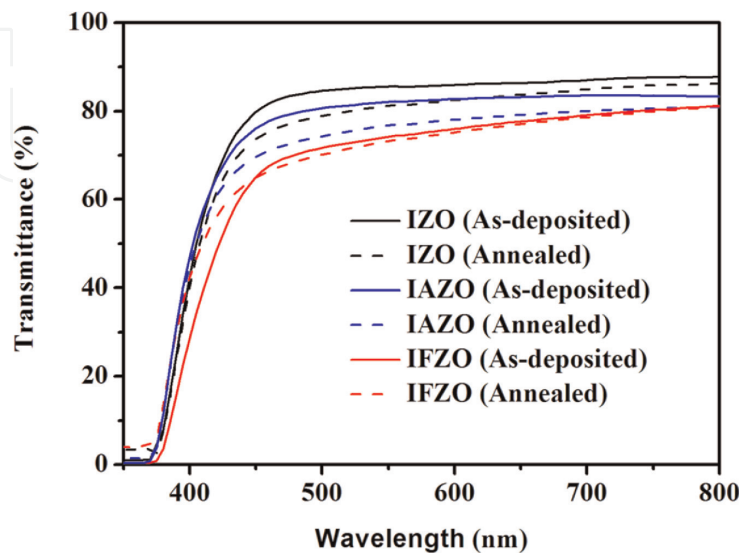


**Figure 11.**
*Transmittance spectra [18].*

with undoped ZnO. The near band emission is observed at 3.22 eV when Y concentration is 0% and 3.30 eV when Y is 5%. The Y creates a screened Coulomb potential field, and the results decrease in the intensity of the near band emission.

The band gap increases with an increase in Al concentration in ZnO films [29]. It leads to shifting of absorption band to UV region due to Burstein-Moss shift. The transmittance of doped and undoped ZnO films increase with wavelength. It has a transmittance of 74% in the blue region and more than 90% in the IR region. The decrease in optical transmittance for Al-doped ZnO, when compared with ZnO, is due to the reduction of grain boundaries. The refractive index and extinction coefficient also decreases due to the doping of 'Al'. The transmission of Sr-doped ZnO thin film is higher than undoped ZnO films [16]. Increasing the molarity of the dopant solution increases the transmission coefficient. The optical band gap and the carrier concentration increases, but the refractive index decreases, and the results are given in **Table 3**.

IZO, IAZO and IFZO films show high transmittance between 70 and 85% in the visible region. The annealing process decreases the transmission for IZO and IAZO films, whereas the transmission increases due to the annealing in the case of IFZO thin films. Moreover, the annealing results in a slight blue shift of the absorption edge. **Figure 11** shows the transmission spectra of as-deposited and annealed IZO, IAZO and IFZO films.

## 4. Electrical properties

ZnO/Si heterojunction diodes show the maximum rectification for 80°C grown ZnO, which has the highest rectification [17]. Such junction has fast ON/OFF

switching ratio up to $10^3$ times/s. When ZnO is prepared at high temperature, the resistivity of the films becomes comparable to the resistivity of the Si substrates. There is no proper variation observed as a function of the preparation temperature of the films. But as the input wavelength of the photon increases, the photoresponsivity increases. **Table 4** gives the photoresponsivity of the ZnO/Si heterojunction for various grown temperatures and various wavelengths of the incident photon at 0.5 V reverse bias condition.

The Co-doped ZnO thin films show the semiconducting nature, and it is confirmed from the relationship between the conductivity and temperature [1]. The conductivity increases as the temperature increases. The conductivity is measured from 340 K, not from room temperature. The non-linear behaviour of the electrical conductivity is due to the lattice defects. The activation energy decreases due to the increase in the donor carrier density as the doping concentration of Co increases in the temperature limit of 363–403 K. But the activation energy increases due to decrease in Fermi level as the doping concentration increases in the temperature limit 408–473 K. The reported activation energy is given in **Table 5**.

In the case of Y-doped ZnO thin films, the electrical resistivity of the film first decreases and then increases as the doping concentration of Y increases [26]. The minimum electrical resistivity of the films is 7.25 ohm-cm, and this value corresponds to the doping concentration of 0.5%. Due to the scattering from grain boundaries and ionized impurities, the Hall mobility decreases gradually from 15.6 to 6.1 cm$^2$ V$^{-1}$ s$^{-1}$. The carrier concentration of both IAZO and IFZO films are higher than IZO films [18]. This is due to the substitution of fluorine ions at oxygen ion site and aluminium ions at zinc site resulting in one free electron per site. Hence the conductivity of both films increases than IZO films. IFZO films have the highest mobility, and IAZO films have the lowest mobility (**Figure 12**).

| | Grown temperature of the heterostructure | | | |
| --- | --- | --- | --- | --- |
| | 80°C | 150°C | 200°C | 250°C |
| λ = 350 nm | 37 mAW$^{-1}$ | 30 mAW$^{-1}$ | 30 mAW$^{-1}$ | 35 mAW$^{-1}$ |
| λ = 475 nm | 74 mAW$^{-1}$ | 80 mAW$^{-1}$ | 80 mAW$^{-1}$ | 74 mAW$^{-1}$ |
| λ = 585 nm | 85 mAW$^{-1}$ | 90 mAW$^{-1}$ | 90 mAW$^{-1}$ | 84 mAW$^{-1}$ |

**Table 4.**
*Photoresponsivity of the ZnO/Si heterojunction.*

| Co doping concentration % | Activation energy | |
| --- | --- | --- |
| | 363–403 K | 403–473 K |
| 0 | 0.405 eV | 0.044 eV |
| 1 | 0.383 eV | 0.077 eV |
| 2 | 0.271 eV | 0.343 eV |
| 4 | 0.119 eV | 0.439 eV |

**Table 5.**
*Activation energy of Co-doped ZnO films.*
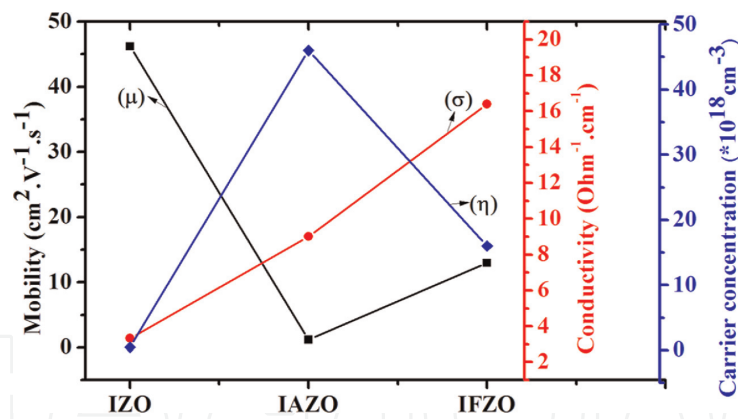
**Figure 12.**
*Mobility, conductivity and carrier concentration of IZO, IAZO and IFZO films [18].*

## 5. Conclusion

This chapter provides an insight into the property tailoring by parameter variations and doping that gives interesting variation in low dimensions for ZnO. Interesting basic properties and wide range of applications encourage the research about undoped and doped ZnO thin film synthesis by both physical and chemical methods. They provide amazing opportunity to include a design with ease to prepare ZnO thin film structures possessing desired electrical and optical properties. Representative works by the author group and few others are reviewed to indicate the variation in structural, optical and electrical properties of undoped and metal-doped ZnO thin films. The co-doped ZnO films are also discussed.

## Author details

Lourdhu Bruno Chandrasekar[1]*, S. Nagarajan[2], Marimuthu Karunakaran[3] and
T. Daniel Thangadurai[4]

1 Department of Physics, The American College, Madurai, India

2 Department of Chemistry, NIT, Imphal, Manipur, India

3 Department of Physics, Alagappa Government Arts College, Karaikudi, India

4 Department of Nanotechnology, Sri Ramakrishna College of Engineering, Coimbatore, India

*Address all correspondence to: brunochandrasekar@gmail.com

**IntechOpen**

11

## References

[1] Saha SK, Rahman MA, Sarkar MRH, Shahjahan M, Khan MKR. Effect of Co doping on structural, optical, electrical and thermal properties of nanostructured ZnO thin films. Journal of Semiconductors. 2015;**36**:033004

[2] Siagian SM, Sutanto H, Permatasari A. Effect of Co doping to the optical properties of ZnO:Co Thin films deposited on glass substrate by sol-gel spray coating technique. Journal of Physics: Conference Series. 2017;**795**: 012009

[3] Ravichandran AT, Karthick R, Xavier AR, Chandrmohan R, Mantha S. Influence of Sm doped ZnO nanoparticles with enhanced photoluminescence and antibacterial efficiency. Journal of Materials Science: Materials in Electronics. 2017;**28**(9): 6643-6648

[4] Emami-Karvani Z, Chehrazi P. Antibacterial activity of ZnO nanoparticle on Gram-positive and Gram-negative bacteria. African Journal of Microbiology Research. 2011;**5**:1368

[5] Sirelkhatim A, Mahmud S, Seeni A, Mkaus NH, Ann LC, Bakhori SKM, et al. Review on zinc oxide nanoparticles: Antibacterial activity and toxicity mechanism. Nano-Micro Letters. 2015; **7**:219

[6] Hou Y, Mei Z, Du X. Semiconductor ultraviolet photodetectors based on ZnO and MgxZn1-xO. Journal of Physics D: Applied Physics. 2014;**47**:283001

[7] Du XY, Fu YQ, Tan SC, Luo JK, Flewitt AJ, Maeng S, et al. ZnO film for application in surface acoustic wave device. Journal of Physics: Conference Series. 2007;**76**:012035

[8] Zhang H, Shen R, Liang H, Liu Y, Yang Liu X, Xia G. n-ZnO/p-GaN heterojunction light-emitting diodes with a polarization-induced graded-p-AlxGa1−xN electron-blocking layer. Journal of Physics D: Applied Physics. 2013;**46**:065101

[9] Chang S, Park H, Cheng JJ, Rekemeyer PH, Gradecak S. Improved efficiency in organic/inorganic hybrid solar cells by interfacial modification of ZnO nanowires with small molecules. Journal of Physics D: Applied Physics. 2014;**47**:394016

[10] Shishiyanu ST, Shishiyanu TS, Lupan OI. Sensing characteristics of tin-doped ZnO thin films as $NO_2$ gas sensor. Sensors and Actuators B. 2005;**107**:379

[11] Dighavkar C. Characterization of nanosized zinc oxide based ammonia gas sensor. Archives of Applied Science Research. 2013;**5**:96

[12] Yakuphanoglu F, Ilican S, Caglar M, Caglar Y. The determination of the optical band and optical constants of non-crystalline and crystalline ZnO thin films deposited by spray pyrolysis. Journal of Optoelectronics and Advanced Materials. 2007;**7**:2180

[13] Li W, Hao H. Effect of temperature on the properties of Al:ZnO films deposited by magnetron sputtering with inborn surface texture. Journal of Materials Science. 2012;**47**:3516. DOI: 10.1007/s10853-011-6196-y

[14] Ilican S, Caglar Y, Caglar M. Polycrystalline indium-doped ZnO thin films: Preparation and characterization. Journal of Optoelectronics and Advanced Materials. 2008;**10**:2578

[15] Shukla G, Khare A. Spectroscopic studies of laser ablated ZnO plasma and correlation with pulsed laser deposited ZnO thin film properties. Laser and Particle Beams. 2010;**28**:149

[16] Vijayan TA, Chandramohan R, Valanarasu S, Thirumalai J, Subramanian SP. Comparative investigation on nanocrystal structure, optical, and electrical properties of ZnO and Sr-doped ZnO thin films using chemical bath deposition method. Journal of Materials Science. 2008; **43**:1776

[17] Alkis S, Tekcan B, Nayfeh A, Okyay AK. UV/Vis range photodetectors based on thin film ALD grown ZnO/Si heterojunction diodes. Journal of Optics. 2013;**15**:105002

[18] Hadri A, Taibi M, El Hat A, Mzerd A. Transparent and conductive Al/F and In co-doped ZnO thin films deposited by spray pyrolysis. Journal of Physics: Conference Series. 2016;**689**: 012024

[19] Wei Y, Wei R, Peng S, Zhuangde J. Effect of annealing temperature of $Bi_{1.5}Zn_{1.0}Nb_{1.5}O_7$ gate insulator on performance of ZnO based thin film transistors. Journal of Semiconductors. 2016;**37**:074007

[20] Zulkifli Z, Sharma S, Shinde S, Kalita G, Tannemura M. Effect of annealing in hydrogen atmosphere on ZnO films for field emission display. Materials Science and Engineering. 2015;**99**:0012030

[21] Lv J, Liu C, Gong W, Zi Z, Chen X, Chen X, et al. Study of near white light emission for ZnO thin films grown on silicon substrates. Semiconductor Science and Technology. 2012;**27**:115021

[22] Jin YP, Zhang B, Wang JZ, Shi LQ. P-type nitrogen-doped ZnO films prepared by in-situ thermal oxidation of $Zn_3N_2$ films. Chinese Physics Letters. 2016;**33**(5):058101

[23] Bruno Chandrasekar L, Karunakaran M, Chandramohan R, Daniel Thangadurai T, Vijayalakshmi R. X-ray peak profile analysis of $Zn_{1-}$

$_yMn_yO$ and $Zn_{1-y}Ni_yO$ nanostructures. Journal of Nanoengineering and Nanomanufacturing. 2016;**6**:217

[24] Bruno Chandrasekar L, Chandramohan R, Chandrasekaran S, Thirumalai J, Vijayalakshmi R. Luminescence and unit cell analysis of $Zn_{1-x}Cd_xO$ nanoparticles. Advanced Science Focus. 2013;**1**:292

[25] Singh K, Shukla DK, Majid S, Dhar R, Choudhary RJ, Phase DM. Structural optical and electronic properties of Fe and Ga doped ZnO thin films grown using pulsed laser deposition technique. Journal of Physics: Conference Series. 2016;**755**:012040

[26] Yu Q, Fu W, Yu C, Yang H, Wei R, Sui Y, et al. Ferromagnetic nanocrystalline Gd-doped ZnO powder synthesized by coprecipitation. Journal of Physics D: Applied Physics. 2007; **40**:5592

[27] Yilmaz M. Characteristic properties of spin coated ZnO thin films: The effect of Ni doping. Physica Scripta. 2014;**89**: 095802

[28] Karunakaran M, Chandramohan R, Balamurali S, Gomathi S, Kabila K, Mahalingam T. Current-voltage characteristics of p-CuO/n-ZnO:Sn solar cell. International Journal of Thin Films Science and Technology. 2014;**3**:61

[29] Chandramohn R, Dhanasekaran V, Ezhilvizhian S, Vijayan TA, Thirumalai J, Peter AJ, et al. Spectral properties of aluminium doped zinc oxide thin films prepared by SILAR method. Journal of Materials Science: Materials in Electronics. 2012;**23**:390

[30] Boukhenoufa N, Mahamdi R, Rechem D. Structural, optical, morphological and electrical properties of undoped and Al-doped ZnO thin films prepared using sol–gel dip coating process. Journal of Semiconductors. 2016;**37**:113001